
MATHEMATICAL MORPHOLOGY ON DIRECTIONAL DATA

Konstantin Hauch

Department of Mathematics,
RPTU Kaiserslautern-Landau,
Kaiserslautern, Germany
hauch@mathematik.uni-kl.de

Claudia Redenbach

Department of Mathematics,
RPTU Kaiserslautern-Landau,
Kaiserslautern, Germany
redenbach@mathematik.uni-kl.de

ABSTRACT

We define morphological operators and filters for directional images whose pixel values are unit vectors. This requires an ordering relation for unit vectors which is obtained by using depth functions. They provide a centre-outward ordering with respect to a specified centre vector. We apply our operators on synthetic directional images and compare them with classical morphological operators for grey-scale images. As application examples, we enhance the fault region in a compressed glass foam and segment misaligned fibre regions of glass fibre reinforced polymers.

Keywords depth function · μ CT imaging · image processing · filtering · glass foam · glass fibre reinforced polymer

1 Introduction

Mathematical morphology combines nonlinear image processing and filtering techniques based on ideas from (random) set theory, topology, and stochastic geometry. It is widely applied for the analysis of spatial structures, e.g. from geology, biology or materials science. The foundations of mathematical morphology are laid in the books by Matheron [1], Serra [2, 3], and Soille [4]. Sternberg [5] generalised mathematical morphology to numerical functions via the umbra method, i.e., the application of set morphology to the graph of the function. Ronse [6] and Goutsias et al. [7] derived a further generalisation to complete lattices, that is, partially ordered sets with the property that all subsets have a supremum and an infimum.

The progress of imaging methods from binary via grey-scale images to vector-valued images, such as colour or ultra-spectral images, requires modified morphological operators. In particular, diffusion tensor imaging (DTI) in neuroimaging [8] results in vector-valued images showing the diffusion of water molecules in the brain. These images can be used to better understand neural diseases as the diffusion in diseased brains is disturbed or altered compared to healthy brains. For instance, Zhang et al. [9] proposed a novel Alzheimer's disease multi-class classification framework with embedding feature selection and fusion based on multi-modal neuroimaging.

In mathematical morphology, the step from univariate to multivariate pixel values involves the challenging task of ordering vectors to define the notions of minimum and maximum of a set of vectors. An ordering structure for vectors can be derived from the concept of depth [10]. For a set of vectors, depth functions assign to each vector a value that measures its "centrality" within the set. The "centre" is the vector maximising the depth function. Thus, a centre-outward ordering based on the depth values of each vector yields a sound definition of minimum and maximum.

Velasco-Forero et al. [11] defined multivariate mathematical morphological operators via random projection depth. They illustrated their approach on colour and hyperspectral images. Concepts of depth for directional data, i.e. unit vectors in \mathbb{R}^d , have been studied, for instance, by Liu et al. [12] and Pandolfo et al. [13]. Ley et al. [14] introduced quantiles for directional data and the angular Mahalanobis depth, and García-Portugués et al. [15] developed optimal tests for rotational symmetry against new classes of hyperspherical distributions.

Based on an ordering on the unit sphere \mathcal{S}^{d-1} , mathematical morphology was extended to directional images by several authors. Roerdink [16] introduced mathematical morphology on the sphere via generalised Minkowski operations. His motivation is morphological processing of earth pictures under consideration of the curvature. Morphological operators for angle-valued images were introduced by Peters [17] and Hanbury et al. [18]. However, a generalisation of their

results to the unit sphere \mathcal{S}^{d-1} with $d > 2$ is not straightforward. Frontera-Pons and Angulo [19] defined morphological operators via a local partial ordering. They used the Fréchet-Karcher barycenter as local origin μ on the sphere. The maximum and minimum of a set of vectors are then found via projecting the vectors into the tangent space at μ . A drawback of their approach is that the minimum and maximum derived this way are not necessarily elements of the given vector set, which seems unnatural. Angulo [20] extended the concept of multi-scale morphological operators, i.e. a scale-dependent morphology and filters, from \mathbb{R} -valued to \mathbb{R}^d -valued images. He defined morphological scale-space operators on metric Maslov-measurable spaces for images supported on point clouds. An application of his operators to RGB-valued point clouds, e.g. for object extraction, showed the usefulness of applying the theory of multi-scale morphological operators to \mathbb{R}^d -valued images.

In this work, we introduce morphological operators on directional images. Section 2 contains basics about mathematical morphology for grey-scale images and statistical depth functions on \mathcal{S}^{d-1} . In Section 3, we introduce the concept of mathematical morphology on directional data using the directional projection depth. These morphological operators are extended to multi-scale operators in Section 4. We illustrate and interpret our findings on synthetic and real-world \mathcal{S}^2 -valued images in Section 5. A short conclusion is given in Section 6.

2 Basics and Notation

2.1 Images

We denote by $\mathcal{S}^{d-1} = \{x \in \mathbb{R}^d : \|x\|_2 = 1\}$ the $(d-1)$ -dimensional unit sphere and $\|x\|_2 = \sqrt{x^T x}$ the Euclidean norm. An image is a mapping $I : E \rightarrow S$ that is defined on a q -dimensional domain E with $E \subset \mathbb{R}^q$ or $E \subset \mathbb{Z}^q$. The set S is the set of pixel values. We call I a binary image if $S = \{0, 1\}$, a grey-scale image if $S \subset \mathbb{R}$, a vector-valued image if $S \subset \mathbb{R}^d$ and a directional (\mathcal{S}^{d-1} -valued) image if $S \subset \mathcal{S}^{d-1}$. Usually, $q, d \in \{2, 3\}$. In this paper, we consider examples of q -dimensional \mathcal{S}^{d-1} -valued images with $q = 2, 3$ and $d = 3$. We denote by

- $\max I$ the maximal possible pixel value of an image I . For instance, $\max I = 1$ if I is a binary image or $\max I = 255$ if I is an 8-bit grey-scale image.
- $\overline{\mathbb{R}} = \mathbb{R} \cup \{-\infty, \infty\}$ the extended real numbers.
- $SO(d)$ the rotation group on \mathbb{R}^d .
- $x \times y$ the cross product between two vectors $x, y \in \mathbb{R}^d$.
- $\mathcal{GC}_{\mu, x} = \{y \in \mathbb{R}^d : (x \times \mu)^T y = 0\} \cap \mathcal{S}^{d-1}$ the great circle containing the vectors μ and $x \in \mathcal{S}^{d-1}$. For $d = 3$, the great circle $\mathcal{GC}_{\mu, x}$ corresponds to a closed curve on the surface of \mathcal{S}^2 created by the intersection of \mathcal{S}^2 and a 2-dimensional hyperplane H passing through the origin 0_3 [21].
- \check{b} the reflection of a function $b : \mathbb{R}^q \rightarrow \overline{\mathbb{R}}$, i.e., $\check{b}(i) = b(-i)$ for all $i \in \mathbb{R}^q$, and by \check{B} the reflection of a set $B \subset \mathbb{R}^q$, i.e., $\check{B} = -B$. A function b is called symmetric if $b = \check{b}$ and a set B is symmetric if $B = \check{B}$.

2.2 Mathematical morphology

We first define morphological operators on grey-scale images I . See [1, 2, 4] for a detailed introduction. The two fundamental operations of mathematical morphology are erosion $\tilde{\varepsilon}_b$ and dilation $\tilde{\delta}_b$. They depend on a structuring function $b : \mathbb{R}^q \rightarrow \overline{\mathbb{R}}$ and are defined as

$$\tilde{\varepsilon}_b(I)(i) = \inf_{j \in E} \{I(j) - b(j - i)\}, \quad i \in E, \quad (1)$$

$$\tilde{\delta}_b(I)(i) = \sup_{j \in E} \{I(j) + b(j - i)\}, \quad i \in E. \quad (2)$$

In the discrete case, supremum and infimum can be replaced by maximum and minimum. We will not discuss edge effects here (see [22]). Throughout the paper, we assume that b is symmetric.

A well-known and widely used example for b is the flat structuring function. Given a structuring element $B \subset \mathbb{R}^q$, it is defined as

$$b(i) = \begin{cases} 0 & i \in B \\ -\infty & i \notin B. \end{cases}$$

We assume that B is centred at the origin and symmetric. Morphological operators with flat structuring functions are called flat operators. Symbols for flat operators will be written with index B rather than b , e.g., a flat erosion with structuring element B is denoted by $\tilde{\varepsilon}_B$.

Non-flat or volumic structuring functions assign non-constant weights to the pixel values [2]. For instance,

$$b(i) = - \left(\frac{\|i\|_2}{2} \right)^2$$

is a non-flat structuring function. Note that the grey-scale ranges of images dilated or eroded by non-flat structuring functions are not bounded [4]. For instance, an erosion with a non-flat structuring function of an image with non-negative pixel values can result in negative pixel values. Flat structuring functions do not suffer from that problem. The output of a flat erosion or dilation is bounded by the grey-scale range of the input image.

The composition of erosion and dilation yields the morphological operators opening $\tilde{\gamma}_b$ and closing $\tilde{\varphi}_b$

$$\tilde{\gamma}_b(I)(i) = \tilde{\delta}_b(\tilde{\varepsilon}_b(I))(i),$$

$$\tilde{\varphi}_b(I)(i) = \tilde{\varepsilon}_b(\tilde{\delta}_b(I))(i).$$

In applications, the opening is used to remove bright noise and the closing to remove dark noise.

Some properties of the morphological operators are summarised in the following, see also [1, 2, 22]. Let $i \in E$, I, I' grey-scale images and $\{I_l\}_{l \in \mathbb{N}}$ a family of grey-scale images. We write $I \leq I'$ if $I(i) \leq I'(i)$ for all $i \in E$. Furthermore, \bigvee denotes the point-wise maximum operator and \bigwedge the point-wise minimum operator.

1. All the morphological operators are non-linear, i.e., in general

$$\tilde{\Psi}(aI + bI') \neq a\tilde{\Psi}(I) + b\tilde{\Psi}(I'),$$

where $a, b \in \mathbb{R}$ and $\tilde{\Psi} = \tilde{\delta}_b, \tilde{\varepsilon}_b, \tilde{\gamma}_b$, or $\tilde{\varphi}_b$.

2. Dilation and erosion are dual w.r.t. complementation \tilde{C} with $\tilde{C}I(i) = \max I - I(i)$, i.e.,

$$\tilde{\delta}_b(I) = \tilde{C}\tilde{\varepsilon}_b(\tilde{C}I)$$

with $b(i) = b(-i)$ due to symmetry.

3. Opening and closing are dual w.r.t. complementation \tilde{C} , i.e.

$$\tilde{\gamma}_b(I) = \tilde{C}\tilde{\varphi}_b(\tilde{C}I)$$

4. Opening and closing are idempotent, i.e.,

$$\tilde{\gamma}_b(\tilde{\gamma}_b(I)) = \tilde{\gamma}_b(I),$$

$$\tilde{\varphi}_b(\tilde{\varphi}_b(I)) = \tilde{\varphi}_b(I).$$

5. The following distribution laws hold

$$\tilde{\delta}_b \left(\bigvee_l I_l \right) = \bigvee_l \tilde{\delta}_b(I_l),$$

$$\tilde{\varepsilon}_b \left(\bigwedge_l I_l \right) = \bigwedge_l \tilde{\varepsilon}_b(I_l).$$

6. Dilation is associative and erosion fulfils the chain rule, i.e.,

$$\tilde{\delta}_b(\tilde{\delta}_{b'}(I)) = \tilde{\delta}_{\tilde{\delta}_b(b')}(I),$$

$$\tilde{\varepsilon}_b(\tilde{\varepsilon}_{b'}(I)) = \tilde{\varepsilon}_{\tilde{\varepsilon}_b(b')}(I).$$

7. All morphological operators are increasing, i.e.,

$$I \leq I' \Rightarrow \tilde{\Psi}(I) \leq \tilde{\Psi}(I'),$$

where $\tilde{\Psi} = \tilde{\delta}_b, \tilde{\varepsilon}_b, \tilde{\gamma}_b$, or $\tilde{\varphi}_b$.

8. If b is defined at the origin and $b(0) \geq 0$, dilation is extensive and erosion is anti-extensive, i.e.,

$$\tilde{\varepsilon}_b(I) \leq I \leq \tilde{\delta}_b(I).$$

9. Closing is extensive and opening is anti-extensive, i.e.,

$$\tilde{\gamma}_b(I) \leq I \leq \tilde{\varphi}_b(I).$$

The latter two properties can be combined to give the ordering relation

$$\tilde{\varepsilon}_b(I) \leq \tilde{\gamma}_b(I) \leq I \leq \tilde{\varphi}_b(I) \leq \tilde{\delta}_b(I). \quad (3)$$

2.3 Morphological scale-space

In the context of mathematical morphology for grey-scale images, erosion and dilation can be written as scale-space operators [2, 23]

$$\tilde{\varepsilon}_{b_t}(I)(i) = \inf_{j \in E} \{I(j) - b_t(j - i)\} \quad (4)$$

$$\tilde{\delta}_{b_t}(I)(i) = \sup_{j \in E} \{I(j) + b_t(j - i)\}, \quad (5)$$

with a scaled structuring function

$$b_t : \mathbb{R}^q \rightarrow \overline{\mathbb{R}}, \quad t \geq 0$$

with scale parameter t . Following [22, p.15], we assume b_t to have the following properties:

1. $\{b_t\}_t$ is a one-parametric family of convex, continuous, symmetric functions and fulfils the semi-group property, i.e.

$$b_t \dot{+} b_s = b_{t+s} \quad t, s \geq 0, \quad (6)$$

where $\dot{+}$, $+$ are group operations [23]. For instance, when choosing b_t to be a flat structuring function with structuring element tB , the group operations are the Minkowski addition and the standard addition in \mathbb{R} :

$$tB \oplus sB = (t + s)B \quad t, s \geq 0.$$

2. b_t is non-positive and monotonically decreasing with a global maximum at the origin of value zero, i.e.,

$$b_t(i) \leq 0 \quad \forall t \geq 0, i \in \mathbb{R}^q, \quad (7)$$

$$b_t(i) \geq b_t(j) \quad \|i\|_2 < \|j\|_2, \quad (8)$$

$$b_t(0) = 0. \quad (9)$$

An example of a non-flat scaled structuring function is the Poweroid structuring function [22, p.14, Def. 5]

$$b_t(i) = -t \left(\frac{\|i\|_2}{t} \right)^a \quad a \geq 0, t > 0. \quad (10)$$

2.4 Directional data

Directional data are given as a set of vectors on the unit sphere \mathcal{S}^{d-1} for some $d \geq 2$. The vector $x = (x_1, \dots, x_d)^T \in \mathcal{S}^{d-1}$ can be represented as a point on the surface of \mathcal{S}^{d-1} . For x in Cartesian coordinates, a representation in angular coordinates for arbitrary d is given in [24].

For $d = 3$, we use the usual notation for spherical coordinates

$$x = x(\phi, \theta) = \begin{pmatrix} \sin(\theta) \cos(\phi) \\ \sin(\theta) \sin(\phi) \\ \cos(\theta) \end{pmatrix} \quad (11)$$

with co-latitude $\theta \in [0, \pi]$ and longitude $\phi \in [0, 2\pi)$. A random vector $X \in \mathcal{S}^2$ can be represented in spherical coordinates by random variables Θ and Φ with realisations θ and ϕ .

2.5 Statistical depth functions

Depth functions are applied in multidimensional non-parametric robust data analysis and establish an ordering relation between vectors. See [10] for a detailed introduction. The literature gives several depth functions, for instance, halfspace depth [25], simplicial depth [26], projection depth [27], spatial depth [28], or the Mahalanobis depth [10]. For defining a depth for directional data, we initially restrict attention to the class \mathcal{F}_μ of distributions on \mathcal{S}^{d-1} with a bounded density that admits a unique modal direction μ . Examples of distributions in \mathcal{F}_μ are the von Mises–Fisher distribution, the Kent distribution or the Bingham distribution [21]. We further assume that μ coincides with the Fisher spherical median [29], that is

$$\mu = \arg \min_{\gamma \in \mathcal{S}^{d-1}} E(\arccos(X^T \gamma)).$$

Ley et al. [14] adapted the definition of a depth function given in [10, Definition 2.1] for directional data as follows.

Definition 2.1. A statistical depth function on \mathcal{S}^{d-1} is a bounded, non-negative mapping $\mathcal{D}(\cdot) : \mathcal{F}_\mu \times \mathcal{S}^{d-1} \rightarrow \mathbb{R}$ satisfying

1. $\mathcal{D}_{F_{AX}}(AX) = \mathcal{D}_{F_X}(X)$ holds for any random vector $X \in \mathcal{S}^{d-1}$ and any rotation matrix $A \in \mathbb{R}^{d \times d}$.
2. $\mathcal{D}_F(\mu) = \sup_{y \in \mathcal{S}^{d-1}} \mathcal{D}_F(y)$ holds for any $F \in \mathcal{F}_\mu$.
3. For any $F \in \mathcal{F}_\mu$, $\mathcal{D}_F(x) \leq \mathcal{D}_F(c(\alpha))$ for the unique geodesic $c : [0, 1] \rightarrow \mathcal{S}^{d-1}$ with $c(0) = \mu$, $c(1) = x$ and $\alpha \in [0, 1]$.
4. $\mathcal{D}_F(-\mu) = 0$ for each $F \in \mathcal{F}_\mu$ where $-\mu$ is the antipodal point of the centre μ .

Property 1 implies that the depth of a vector should be independent of the underlying coordinate system. Property 2 means that for any F with unique centre μ , the depth function is maximal at μ . Property 3 indicates that for any point X moving away from the centre μ along any geodesic starting at μ , the depth of X decreases monotonically. Property 4 implies that the depth value of X is zero at $-\mu$ since $-\mu$ is at maximal distance from μ on \mathcal{S}^{d-1} .

Depth functions for directional data are, for instance, directional distance-based depths [13] or the angular Mahalanobis depth [14]. For defining morphological operators, we cannot use the latter since its application violates the ordering property (3) for morphological operators. We rather use a re-scaled version of the cosine distance depth from [13] as defined in the following.

2.6 The angular projection depth

Let $X, X_1, \dots, X_n \in \mathcal{S}^{d-1}$ be i.i.d. random vectors with $X \sim F \in \mathcal{F}_\mu$. We define a depth for directional data by

$$D_F^{proj}(X) = \frac{1 + X^T \mu}{2}, \quad X \in \mathcal{S}^{d-1}. \quad (12)$$

$D_F^{proj}(X)$ provides a centre-outward ordering with $D_F^{proj}(\mu) = 1$, $D_F^{proj}(-\mu) = 0$ and is decreasing on a geodesic from μ to $-\mu$. Let $A \in \mathbb{R}^{d \times d}$ be any rotation matrix. Then the distribution of the transformed vector AX has centre $A\mu$. It follows that

$$\begin{aligned} D_{F_{AX}}^{proj}(AX) &= \frac{1 + (AX)^T A\mu}{2} = \frac{1 + X^T A^T A\mu}{2} \\ &= \frac{1 + X^T \mu}{2} = D_F^{proj}(X). \end{aligned}$$

Thus, the properties of a directional depth function given in Definition 2.1 are fulfilled.

The empirical angular projection depth reads

$$D^{proj}(x) = \frac{1 + x^T \hat{\mu}}{2},$$

where $\hat{\mu}$ is the empirical Fisher spherical median [29]

$$\hat{\mu} = \arg \min_{\gamma \in \mathcal{S}^2} \sum_{i=1}^N \arccos(X_i^T \gamma). \quad (13)$$

3 Mathematical morphology on directional images using directional projection depth

The definition of the standard operators of mathematical morphology requires an ordering relation between pixel values, see (1) and (2). Multivariate extensions of ordering and mathematical morphology were subject to several studies [30, 31, 32, 7, 33]. In particular, orderings can be derived from depth functions.

For \mathcal{S}^{d-1} valued images, we use the projection depth D^{proj} to define an ordering relation between unit vectors. This allows for a definition of erosion, dilation, and the morphological operators derived from them as described below. For simplicity, we concentrate on flat morphological operators with structuring element B . In a given application, the assumption $I(i) \sim F \in \mathcal{F}_\mu$ may not be fulfilled. Nevertheless, a suitable central direction μ may be derived from the experimental setup. Hence, μ will be interpreted as a parameter in the following. We will write D_μ^{proj} for the projection

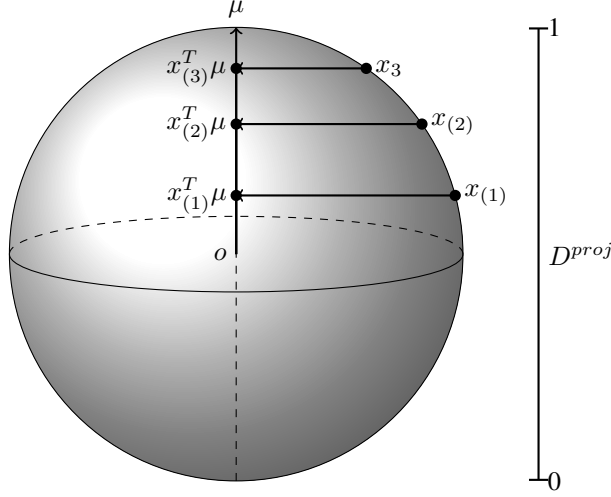


Figure 1: Vector ordering by directional projection depth.

depth using $\mu \in \mathcal{S}^{d-1}$ as the centre. The parameter μ can be selected globally for the whole image or in a locally adaptive manner for parts of the image. The latter is not considered here.

The erosion ε_B of a directional image I at pixel position $i \in E$ is (implicitly) defined by

$$D_\mu^{proj}(\varepsilon_B(I))(i) = \tilde{\varepsilon}_B(D_\mu^{proj}(I))(i),$$

where $\tilde{\varepsilon}$ is the flat erosion of a grey-scale image. Analogously, the dilation δ_B of a directional image I at pixel position $i \in E$ is (implicitly) defined by

$$D_\mu^{proj}(\delta_B(I))(i) = \tilde{\delta}_B(D_\mu^{proj}(I))(i),$$

where $\tilde{\delta}$ is the flat dilation of a grey-scale image. Hence, a dilation will select the most central direction covered by the structuring element while an erosion selects the most outlying direction.

The explicit definition reads

$$\begin{aligned} \varepsilon_B(I)(i) &= D_\mu^{proj-1}(\tilde{\varepsilon}_B(D_\mu^{proj}(I)))(i), \\ \delta_B(I)(i) &= D_\mu^{proj-1}(\tilde{\delta}_B(D_\mu^{proj}(I)))(i), \end{aligned}$$

where D_μ^{proj-1} refers to the preimage under D_μ^{proj} .

As D_μ^{proj} is not injective, the preimage may consist of more than one element. Consider vectors $x_1, x_2 \in \mathcal{S}^{d-1}$ with $x_1^T \mu = x_2^T \mu$. Then, $D_\mu^{proj}(x_1) = D_\mu^{proj}(x_2)$ but $x_1 = x_2$ is not necessarily the case. To resolve this issue we use a lexicographic order for vectors of the same depth value which yields a total ordering [11]. Rotate the vectors such that $\mu = (0, 0, 1)^T$. Among the (pairwise different) vectors $\{x_i\}_{i=1, \dots, n}$ with $D_\mu^{proj}(x_i) = D_\mu^{proj}(x_j)$, we choose the vector x^* with the smallest longitude angle, i.e., $x^* = \arg \min_{x_i} \phi_i$ with (θ_i, ϕ_i) spherical coordinates of x_i , $i = 1, \dots, n$.

Then rotate x^* back.

Opening and closing are defined by

$$\begin{aligned} \gamma_B(I)(i) &= \delta_B(\varepsilon_B(I))(i), \\ \varphi_B(I)(i) &= \varepsilon_B(\delta_B(I))(i). \end{aligned}$$

The theory of h -orderings [7] immediately implies that the operators defined above fulfil the properties of morphological operators stated in Subsection 2.2, see [30]. In this theory, h is a map from \mathcal{S}^{d-1} into a space with a partial order. Here we choose $h = D_\mu^{proj}$.

Of course, further morphological filters have their depth analogy. For instance, the scalar difference between the depth of dilation and erosion defines the morphological gradient

$$\mathfrak{g}_{D_\mu^{proj}, B}(I)(i) = D_\mu^{proj}(\delta_B(I)(i)) - D_\mu^{proj}(\varepsilon_B(I)(i)).$$

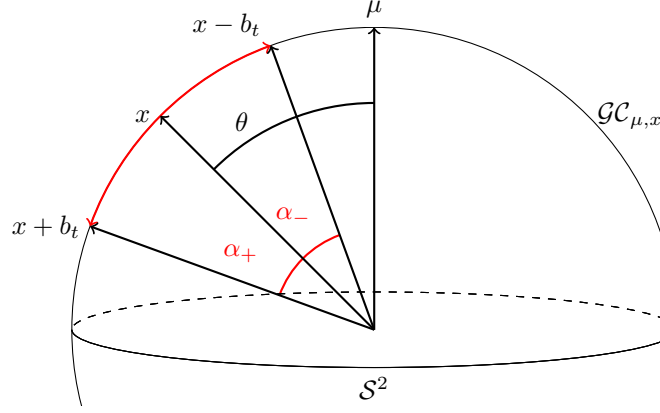


Figure 2: Illustration of the operations $x - b_t$ given in (18) and $x + b_t$ given in (19) with $d = 3$ and $x = x(\phi, \theta)$ in spherical coordinates (11). $x + b_t$ increases the geodesic distance between x and μ by α_+ . $x - b_t$ decreases the geodesic distance between x and μ by α_- . x moves on the great circle $\mathcal{GC}_{\mu, x}$.

The morphological Laplacian is defined by

$$\Delta_{D_\mu^{proj}, B}(I)(i) = \Delta_\delta(i) - \Delta_\varepsilon(i)$$

with $\Delta_\delta(i) = D_\mu^{proj}(\delta_B(I)(i)) - D_\mu^{proj}(I)(i)$ and $\Delta_\varepsilon(i) = D_\mu^{proj}(I)(i) - D_\mu^{proj}(\varepsilon_B(I)(i))$. The shock filter is defined by

$$\text{sf}_{D_\mu^{proj}, B}(I)(i) = \begin{cases} \varepsilon_B(I)(i) & \Delta_{D_\mu^{proj}, B}(I)(i) < 0, \\ \delta_B(I)(i) & \Delta_{D_\mu^{proj}, B}(I)(i) > 0, \\ I(i) & \text{otherwise.} \end{cases}$$

Shock filtering is used to enhance edges. For grey-scale images, the idea is to dilate near local maxima and erode near local minima. This way, the contrast between regions of pixel values with high and low depth is enhanced.

4 Pseudo morphological multi-scale operators for directional images

In the next step, we want to extend morphological operators to a multi-scale setting, leading to a morphological scale space (see [20]). A very simple approach to scaling is scaling of a flat structuring element B by a factor t . Here, we will consider an alternative approach which yields a structuring function which has a meaningful interpretation, fulfils the semi-group property (at least partially), and results in bounded non-flat operators. We call them pseudo morphological operators since their behaviour reminds of erosion and dilation as demonstrated in Section 5.

4.1 Structuring function for directional images

In general, structuring functions $b_t : E \rightarrow \overline{\mathbb{R}}$ are unbounded. Thus, multi-scale dilation and erosion inherit this unboundedness if we use $D_\mu^{proj}(I(i)) + b_t(i)$ and $D_\mu^{proj}(I(i)) - b_t(i)$, respectively. However, we cannot associate a vector with a depth value outside $[0, 1]$ since no unit vector could be found as preimage. In our approach we therefore use structuring functions $b_t : E \rightarrow SO(d)$. We will define the operation $I(i) + b_t(i)$ and $I(i) - b_t(i)$ to be a vector rotation of $I(i)$ where the rotation angle depends on the scale t . Therefore, the depths of $I(i) + b_t(i)$ and $I(i) - b_t(i)$ are both bounded.

The main idea is to rotate a pixel value $x = I(i)$, $i \in E$, about $x \times \mu$ towards μ or away from μ on a great circle $\mathcal{GC}_{\mu, x}$. This increases or decreases the depth value of the rotated x which gives our approach also a meaningful interpretation. Note that $I(i) + b_t(i)$ and $I(i) - b_t(i)$, $i \in E$, result again in directional images which seems natural.

For a formal definition, let $\mu \in \mathcal{S}^{d-1}$, $i \in E$, $x = I(i) \in \mathcal{S}^{d-1}$ with $x^T \mu = \cos(\theta)$ and $R_{\mu, x}(\alpha) \in SO(d)$ be a rotation matrix which rotates x about the cross product $\mu \times x$ and $R_{\mu, x}(\theta)x = \mu$. We define a structuring function b_t for directional images by a mapping

$$\begin{aligned} b_t : E &\rightarrow SO(d) \\ i &\mapsto b_t(i) := R_{\mu, x}(\alpha_t(i)), \end{aligned} \tag{14}$$

with rotation angle $\alpha_t(i)$, $t \geq 0$.

Since $R_{\mu,x}$ depends on x , the structuring function is locally adaptive. We choose

$$\alpha_t(i) = \min \left(\frac{\|i\|_2^2}{t}, \pi \right), \quad (15)$$

where the truncation at π is discussed in more detail in Remark 1. Note the similarity of α_t with quadratic scaling as discussed in [34].

Let $f \square g$ be the infimal convolution of two functions $f, g : \mathbb{R}^q \rightarrow \mathbb{R}$ [35], i.e.,

$$(f \square g)(i) = \inf_{j \in \mathbb{R}^q} \{f(i-j) + g(j)\}. \quad (16)$$

Define

$$(b_t \dot{+} b_s)(i) := R_{\mu,x}((\alpha_t \square \alpha_s)(i)). \quad (17)$$

The structuring element b_t fulfils the semi-group property (6), i.e. $b_t(i) \dot{+} b_s(i) = b_{t+s}(i)$, for $\|i\|_2^2/t, \|i\|_2^2/s < \pi$ as shown in the Appendix.

We illustrate the construction for $d = 3$ and $x = x(\phi, \theta)$ in spherical coordinates as given in (11): The rotation matrix $R_{\mu,x}$ rotates x on the great circle $\mathcal{GC}_{\mu,x}$. We use $R_{\mu,x}$ to move a pixel value $x \in \mathcal{S}^2$ towards μ or away from μ on $\mathcal{GC}_{\mu,x}$. Thus, the rotation matrix $R_{\mu,x}$ causes a change of the angle between x and μ , here the co-latitudinal angle θ . The longitude angle ϕ is not changed. Therefore, we define a rotation of the vector x depending on the structuring function b_t to this change of θ as follows (see Figure 2):

$$x(\phi, \theta) - b_t(i) := x(\phi, \theta - \alpha_-) \quad (18)$$

with

$$\alpha_- = \begin{cases} \alpha_t(i), & \text{for } \alpha_t(i) \in [0, \theta] \\ \theta, & \text{for } \alpha_t(i) > \theta. \end{cases}$$

$$x(\phi, \theta) + b_t(i) := x(\phi, \theta + \alpha_+) \quad (19)$$

with

$$\alpha_+ = \begin{cases} \alpha_t(i), & \text{for } \alpha_t(i) \in [0, \pi - \theta] \\ \pi - \theta, & \text{for } \alpha_t(i) > \pi - \theta. \end{cases}$$

$x - b_t$ has a smaller geodesic distance to μ than x , and $x + b_t$ has a larger geodesic distance to μ than x .

Remark 1 (Truncation of rotation). *The restriction of α_- to θ and of α_+ to $\pi - \theta$ are necessary to achieve an analogous ordering relation as in (3). Otherwise, x can be rotated beyond μ which would decrease $D_\mu^{proj}(x - b_t(i))$. Analogously, x can be rotated beyond $-\mu$ which would increase $D_\mu^{proj}(x + b_t(i))$. To avoid this, we fix the vector at μ or $-\mu$ respectively, such that no rotation beyond is possible.*

With truncation, the semi-group property is no longer valid. However, truncation ensures that

$$D_\mu^{proj}(x + b_t) \leq D_\mu^{proj}(x) \leq D_\mu^{proj}(x - b_t). \quad (20)$$

We obtain (in some sense) analogue properties to (7)–(9):

1. b_t is non-positive w.r.t. D_μ^{proj} in the sense that for rotations of x away from μ its depth decreases, i.e.

$$D_\mu^{proj}(x + b_t(i)) - D_\mu^{proj}(x) \leq 0.$$

2. b_t is monotonically decreasing w.r.t. D_μ^{proj} in the sense that for increasing distance between pixel positions the depth decreases, i.e.

$$D_\mu^{proj}(x + b_t(i)) \geq D_\mu^{proj}(x + b_t(j)), \quad \|i\|_2 < \|j\|_2.$$

3. b_t has a global maximum at the the origin $o \in \mathbb{R}^q$ w.r.t. D_μ^{proj} with

$$D_\mu^{proj}(x + b_t(o)) = D_\mu^{proj}(x)$$

4.2 Pseudo morphological multi-scale operators for directional images

Let b_t be as in Equation (14). The multi-scale erosion ε_{b_t} of a directional image I at pixel position $i \in E$ is (implicitly) defined by

$$D_\mu^{proj}(\varepsilon_{b_t}(I))(i) = \inf_{j \in E} \{D_\mu^{proj}(I(j) - b_t(j - i))\}, \quad (21)$$

where $I(j) - b_t(j - i)$ is defined in Equation (18). Analogously, the multi-scale dilation δ_{b_t} of a directional image I at pixel position $i \in E$ is (implicitly) defined by

$$D_\mu^{proj}(\delta_{b_t}(I))(i) = \sup_{j \in E} \{D_\mu^{proj}(I(j) + b_t(j - i))\}, \quad (22)$$

where $I(j) + b_t(j - i)$ is defined in Equation (19). The interpretation of the multi-scale operators is as follows: We want to rotate the vector $I(j)$ depending on $\|i - j\|_2$ and the scale t towards μ (D_μ^{proj} increases) or towards $-\mu$ (D_μ^{proj} decreases).

Multi-scale opening, closing, morphological gradient and shock filter can be defined as analogues to their flat counterparts.

5 Examples

In this section, we investigate the effect of the morphological operators on synthetic S^2 -valued images and compare them to their standard grey-scale counterparts. As real application examples, we detect misaligned regions in a glass fibre reinforced composite and enhance changes in the displacement field of a compressed glass foam.

5.1 Flat morphological operators

To investigate the newly defined flat morphological operators, we generate a 2-dimensional S^2 -valued image I mimicking direction vectors obtained from two fibres on a homogeneous background. That is, we assume that the image contains two objects consisting of vectors with a small angular deviation from μ , see Figure 3. In the following, we will interpret those as foreground. The background is formed by vectors directed along a plane perpendicular to μ . Flat dilation and flat erosion (Figure 4) show similar behaviour as their standard grey-scale counterparts. Dilation expands objects directed along μ . That is, the directions of background pixels that are close to the edge of these objects are rotated towards μ . An erosion shrinks objects, i.e., object vectors at the edge are rotated so that they are assigned to the image background.

In a similar manner, the flat opening removes foreground objects that are smaller than the structuring element. Figure 4 reveals that object vectors in an object of size smaller than the structuring element B are rotated such that we assign them to the image background. The flat closing removes small holes in the foreground. Vectors with large angular deviation from μ within a background object of size smaller than B are rotated to become part of the image foreground.

The results of shock filtering of I are shown in Figure 5. The edges between the two objects and the background pixels are enhanced.

5.2 Pseudo morphological multi-scale operators

We illustrate the multi-scale dilation and erosion on a directional image I . $\delta_{b_t}(I)$ and $\varepsilon_{b_t}(I)$ behave like their grey-scale counterparts: Figure 6 shows that $\delta_{b_t}(I)$ enlarges objects in the foreground and Figure 7 shows that $\varepsilon_{b_t}(I)$ shrinks objects in the foreground. Of course, the enlargement and shrinkage depend on the continuous scale parameter t .

5.3 Segmentation of aligned and misaligned fibre regions of glass fibre reinforced polymers

Glass fibre reinforced polymers (GFRP) are frequently used in lightweight construction of, e.g., cars, planes, and wind power plants. In civil engineering, they have emerged as an alternative to steel reinforcement as they do not corrode in aggressive conditions such as marine environments [36]. GFRP materials are anisotropic and characterised by high tensile strength in the direction of the reinforcing fibres. When manufactured by injection moulding, the fibres follow the injection direction. However, the fibre orientation in a central layer differs depending on the production parameters. Analysing fibre orientation and quantifying misalignment, for instance by directional filtering [37], may help to optimise the production process and to improve GFRP.

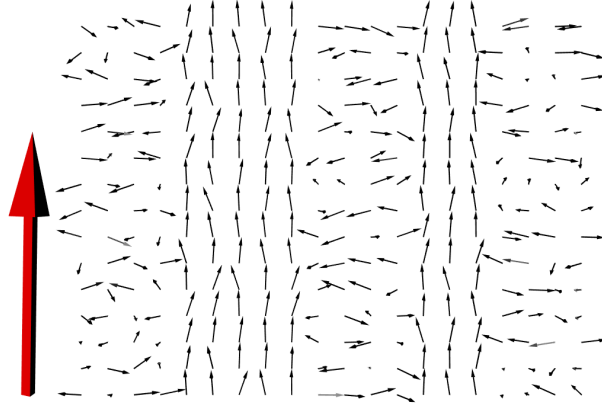


Figure 3: Original S^2 -valued image I . The direction vectors within the fibres are rotationally symmetric around μ (large red vector). Their angular deviation from μ is uniformly drawn from $(0, \pi/8)$. Background vectors are also rotationally symmetric around μ . Their angular deviation from μ is uniformly drawn from $[3/8\pi, 5/8\pi]$.

We examine a μ CT image of GFRP produced and imaged by the Leibniz Institute for Composite Materials (IVW) in Kaiserslautern (Germany) and discussed in [38]. See Figure 8a for an illustration. Pixel-wise fibre orientations can be determined by using partial second derivatives as described in [39] resulting in an S^2 -valued image.

Our goal is to segment the region aligned along the injection direction, as desired, and the misaligned fibre region. Figure 8b shows a grey value encoding of the scalar product between the pixelwise fibre directions and μ . The correctly aligned regions are at the left and right borders while fibres in the central part are misaligned. The higher the value (brighter the image pixel), the more aligned the vectors are along μ . Simply thresholding this image results in a very noisy segmentation. Therefore, the directional image is smoothed prior to the segmentation by a morphological closing along $\mu = (0, 1, 0)$ with B a $7 \times 7 \times 7$ cube.

We choose a threshold value of 1.5 to segment areas aligned along μ , see Figure 8b.

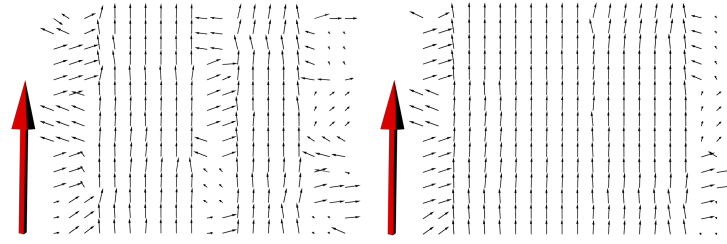
5.4 Enhancement of fault zones in compressed glass foam

To characterise the structural behaviour of complex materials during loading, mechanical tests and simultaneous μ CT imaging (in situ CT) can be used to estimate local displacements of the material on the micro-scale. We analyse a glass foam which consists of very thin struts.

The μ CT images were recorded while the glass foam was compressed in the z-direction. The foam is expected to fail very suddenly due to its thin struts. Nogatz et al. [40] computed the displacement field for the transition from strain level 1% to 3.8% which is shown in Figure 9a. During compression, a fault zone forms which is now post-processed by directional morphology. To this end, our operators are applied to the directional component of the displacement vectors. That is, the vectors were normalised for the calculation of the morphological operators and were subsequently scaled back to their original length. As we mostly expect compression along the loading direction, we choose $\mu = (0, 0, 1)$.

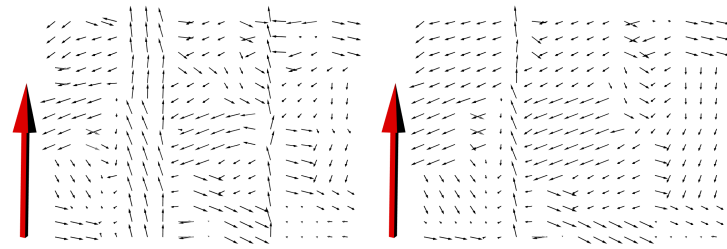
We enhance the fault zone with the morphological gradient, see Figure 9b. If motion estimation algorithms fail to reconstruct these sharp edges, we can enhance them by erosion, as shown in Figure 9c. Some other materials however are known to show creep before failure. Here, a smoother transition seems more reasonable, which is obtained by a dilation, see Figure 9d.

Closing (Figure 9e) and opening (Figure 9f) remove misalignment in the transition between the two regions.



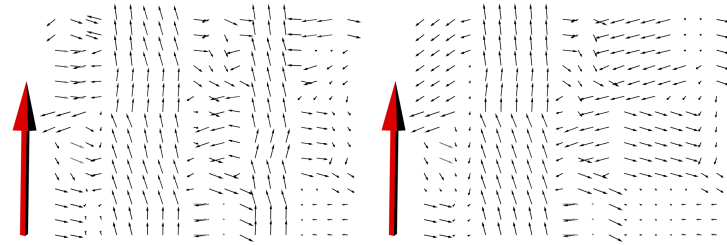
(a) $\delta_B(I)$, B is 3×3

(b) $\delta_B(I)$, B is 5×5



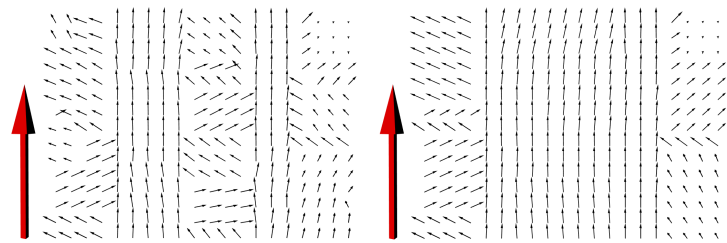
(c) $\varepsilon_B(I)$, B is 3×3

(d) $\varepsilon_B(I)$, B is 5×5



(e) $\gamma_B(I)$, B is 3×3

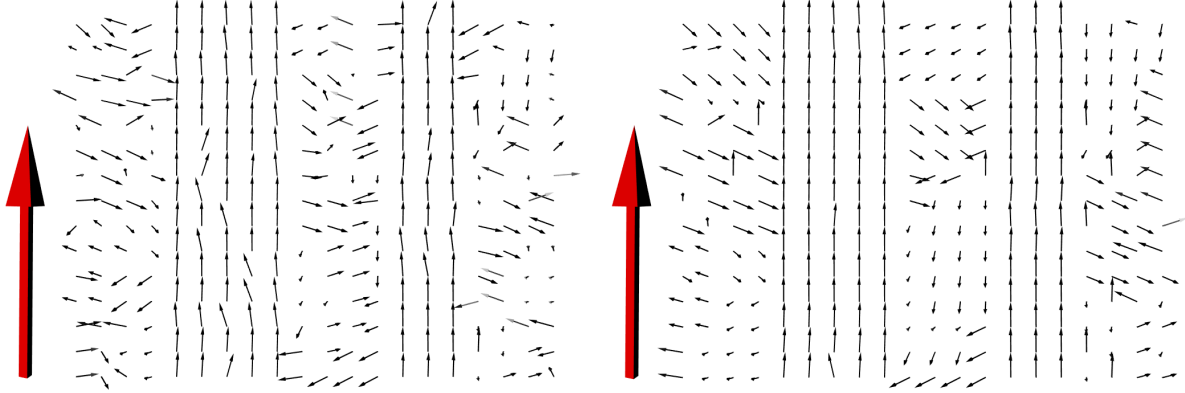
(f) $\gamma_B(I)$, B is 5×5



(g) $\varphi_B(I)$, B is 3×3

(h) $\varphi_B(I)$, B is 5×5

Figure 4: Flat dilation δ_B (a,b), flat erosion ε_B (c,d), flat opening γ_B (e,f) and flat closing φ_B (g,h) with B a square as a structuring element. The large red vector corresponds to μ .



(a) $\text{sf}_B(I)$, B is 3×3

(b) $\text{sf}_B(I)$, B is 5×5

Figure 5: Flat shock filter $\text{sf}_B(I)$ with B a square as structuring element.

6 Conclusion

We have defined morphological operators for \mathcal{S}^{d-1} -valued images. The required ordering for unit vectors is derived from the angular projection depth which enables a sound definition of \mathcal{S}^{d-1} -valued morphological operators and filters. Relations of these morphological operators to their grey-scale counterparts are emphasised. Additionally, we segmented misaligned fiber regions of glass fiber reinforced polymers and enhanced the fault region in a compressed glass foam.

Future work could address the removal of disturbances or the highlighting of directional changes in DTI images by morphological operations [8, 9].

Acknowledgment

We thank Tessa Nogatz for providing the displacement field of the glass foam and Tin Barišin for providing the glass fibre reinforced polymers images.

Appendix

Given (17) the structuring element b_t fulfils the semi-group property (6) for

$$\frac{\|i\|_2^2}{t}, \frac{\|i\|_2^2}{s} < \pi \quad (23)$$

as follows: Let \overline{oi} be the line segment from the origin $o \in \mathbb{R}^q$ to $i \in \mathbb{R}^q$. For $t, s > 0$, let j^* be a point on $\overline{oi} \subset \mathbb{R}^q$ such that

$$\|j^*\|_2 = \frac{s}{t+s} \|i\|_2 \quad (24)$$

$$\|i - j^*\|_2 = \frac{t}{t+s} \|i\|_2. \quad (25)$$

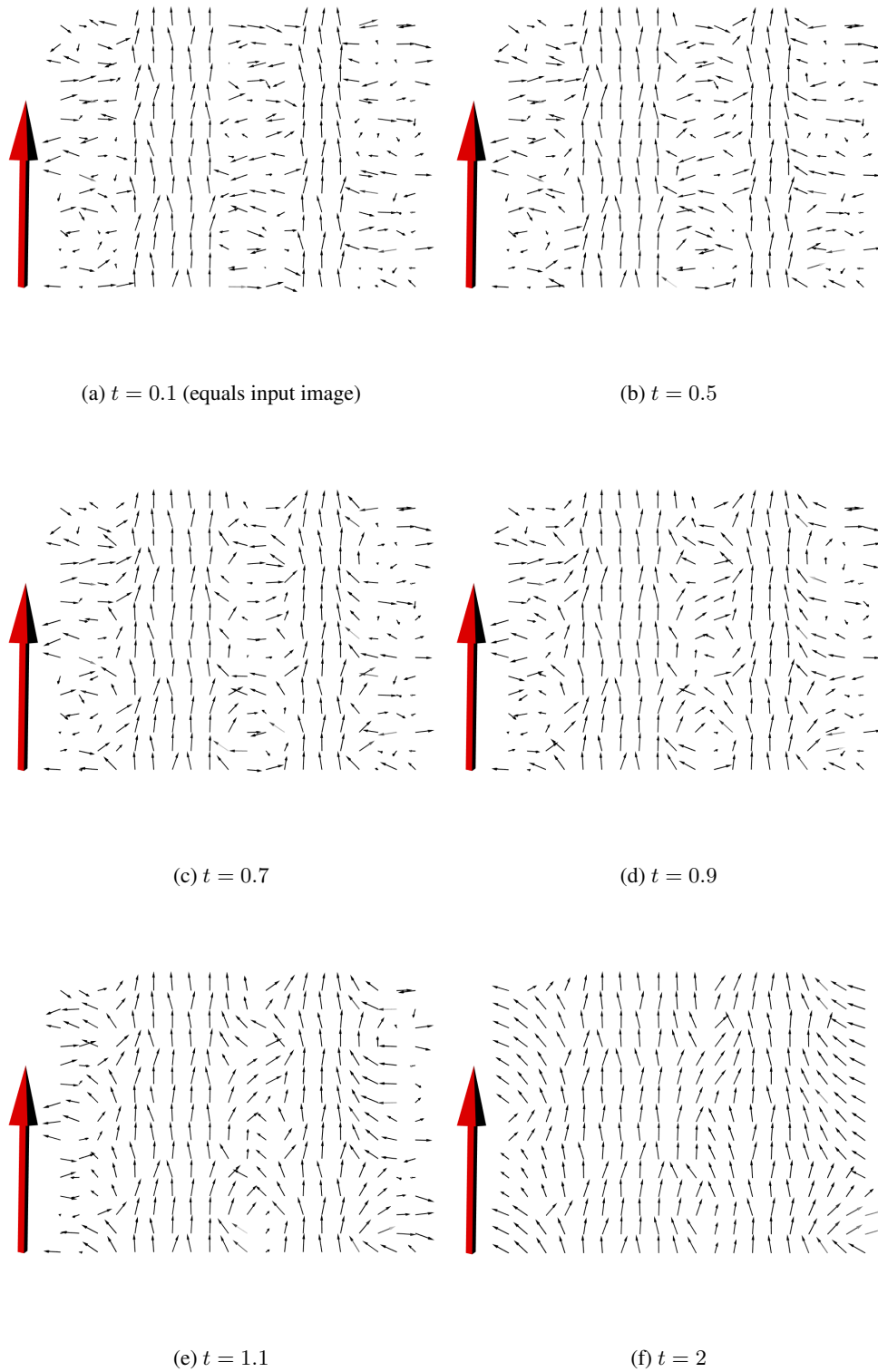


Figure 6: $\delta_{b_t}(I)$ at scales $t = 0.1, 0.5, 0.7, 0.9, 1.1, 2$. The large red vector corresponds to μ .

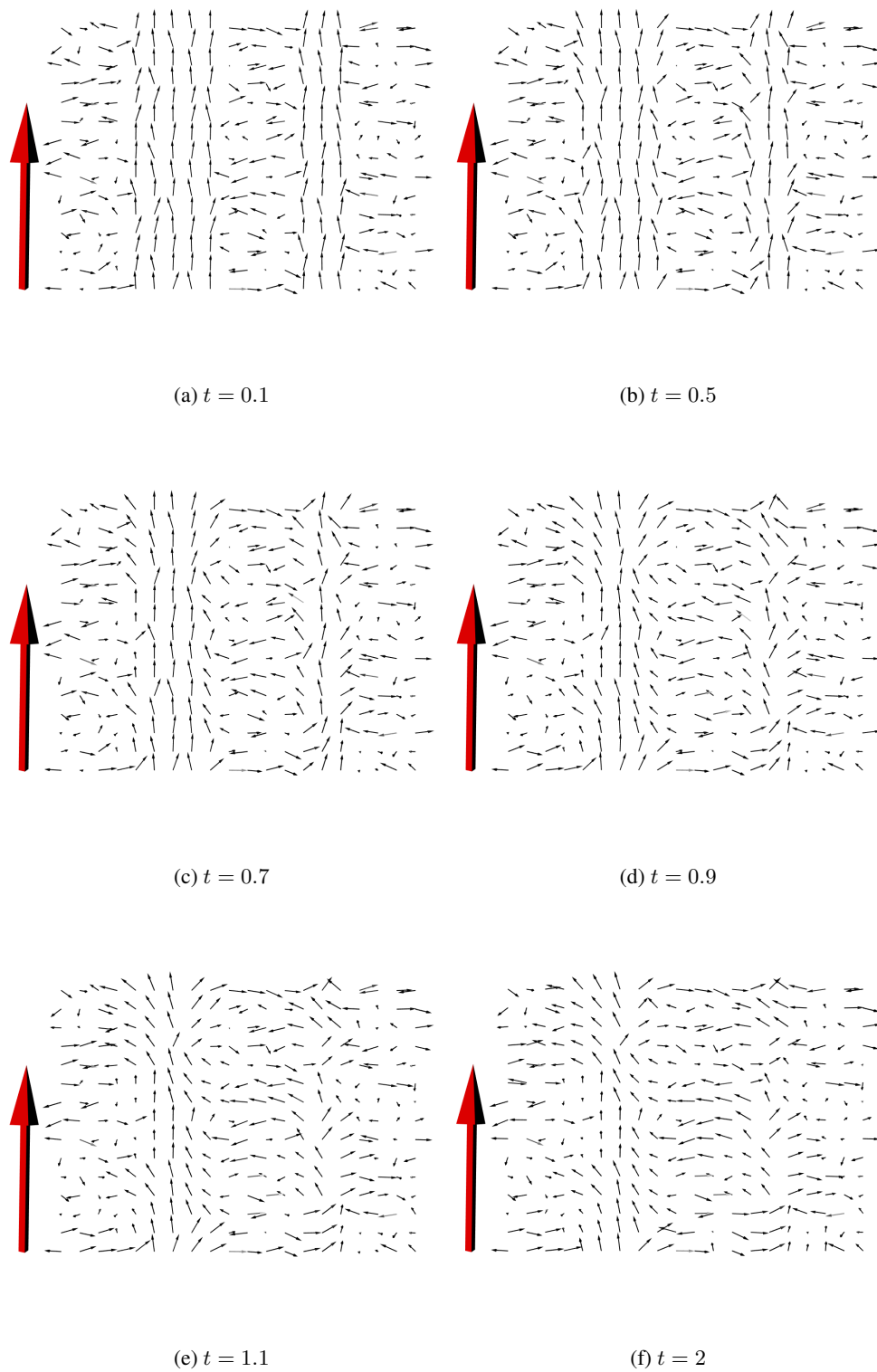
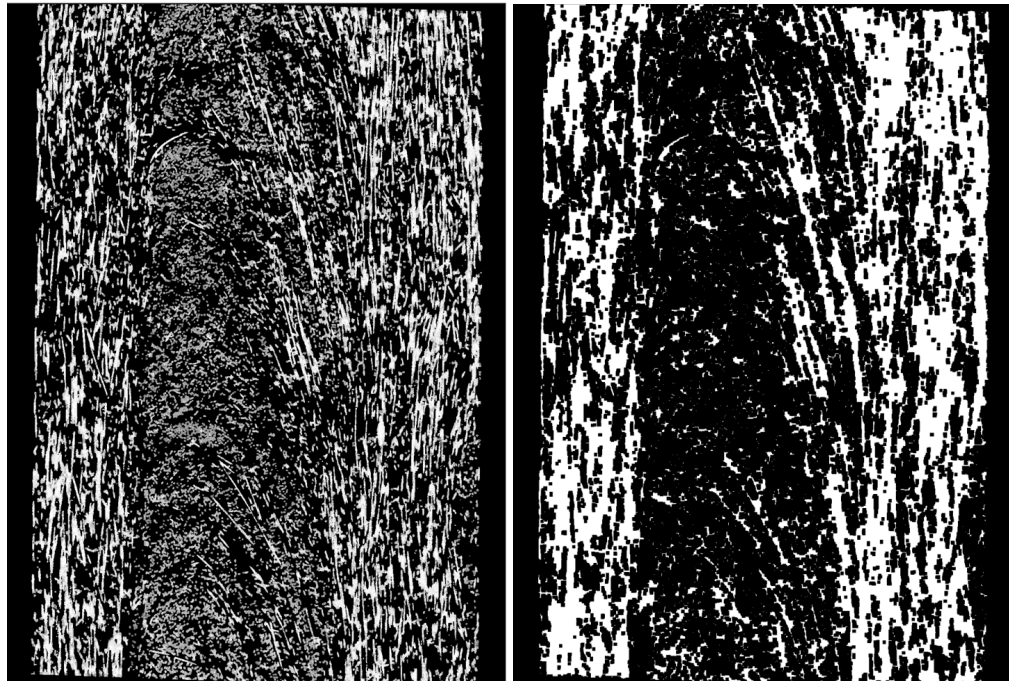


Figure 7: $\varepsilon_{b_t}(I)$ at scales $t = 0.1, 0.5, 0.7, 0.9, 1.1, 2$. The large red vector corresponds to μ .



(a) 2D slice of the original reconstructed 3D μ CT image. The image size is 1100×500 pixels with a pixel spacing of $4 \mu\text{m}$.



(b) Left: 2D slice of a 3D grey scale image encoding the angular deviation of the fibre direction in each pixel from $\mu = (0, 1, 0)$. The left and right side are aligned with μ (correctly aligned). In the inner region, the fibres are misaligned. Right: Closing of the directional image (with B a $7 \times 7 \times 7$ cube) and binarisation of the resulting angular deviation image (threshold 1.5) highlight the correctly aligned areas. The image size is 1100×1500 pixels.

Figure 8: Sectional μ CT image of GFRP produced and imaged by the Leibniz Institute for Composite Materials (IVW) in Kaiserslautern (Germany), the corresponding original and closed directional image.

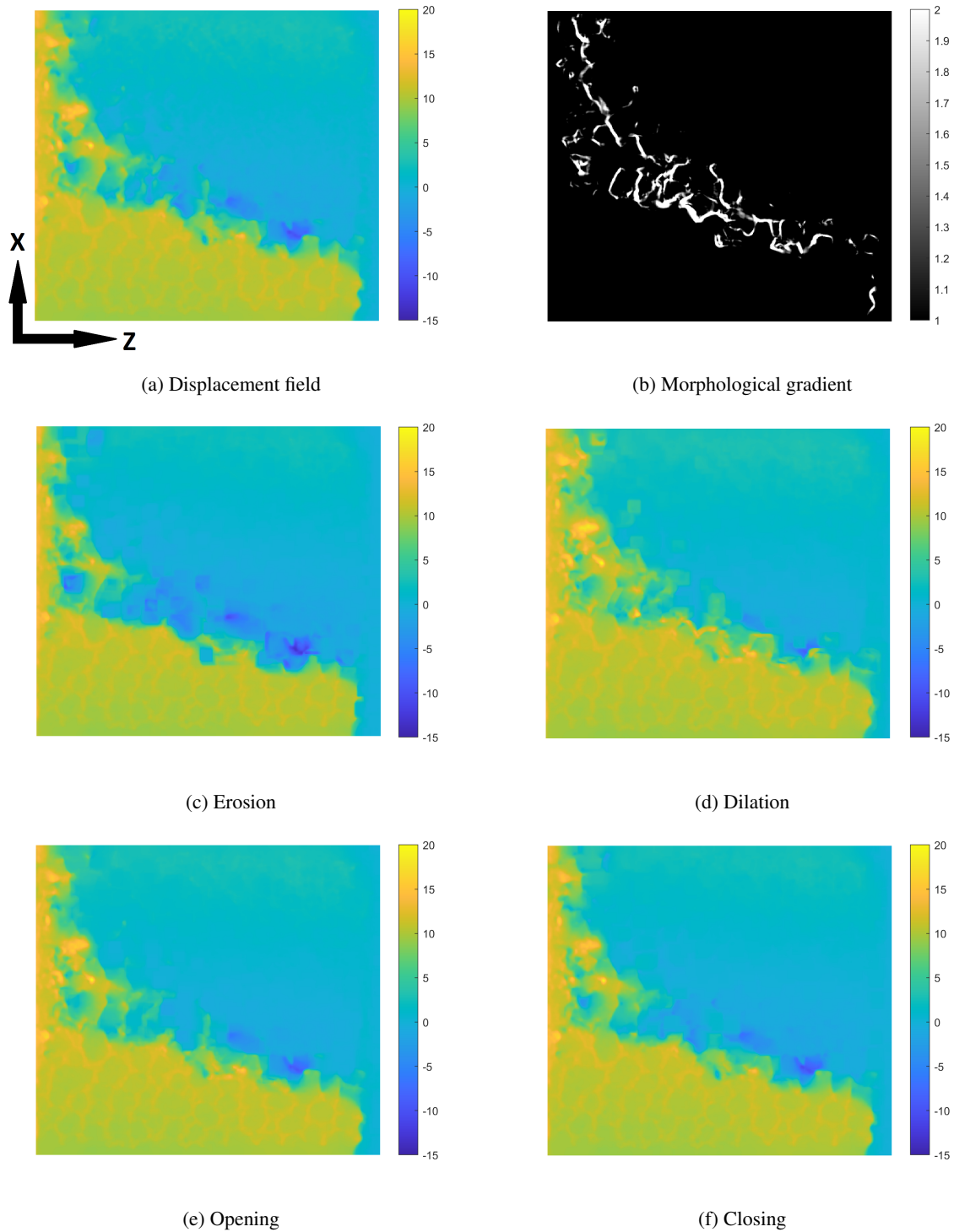


Figure 9: XZ-slices of displacement field based on [40]. Yellow colour indicates movement along the z-direction, and blue refers to the opposite direction. The computed displacement field reflects the influence on the microstructure during compression (a). The morphological gradient (with B a 3×3 square) enhances the fault zone (b). The results of other morphological operators are given in (c-f). We chose B as a 15×15 square.

Then,

$$\begin{aligned}
 (\alpha_t \square \alpha_s)(i) &\stackrel{(16)}{=} \inf_{j \in \mathbb{R}^q} \{ \alpha_t(i - j) + \alpha_s(j) \} \\
 &\stackrel{(15)}{=} \inf_{j \in \mathbb{R}^q} \left\{ \min \left(\frac{\|i - j\|_2^2}{t}, \pi \right) + \min \left(\frac{\|j\|_2^2}{s}, \pi \right) \right\} \\
 &\stackrel{(23)}{=} \inf_{j \in \mathbb{R}^q} \left\{ \frac{\|i - j\|_2^2}{t} + \frac{\|j\|_2^2}{s} \right\} \\
 &\stackrel{j^* \in \overline{oi}}{=} \frac{\|i - j^*\|_2^2}{t} + \frac{\|j^*\|_2^2}{s} \\
 &\stackrel{(24),(25)}{=} \frac{t\|i\|_2^2}{(t+s)^2} + \frac{s\|i\|_2^2}{(t+s)^2} \\
 &= \frac{\|i\|_2^2}{(t+s)} \\
 &\stackrel{(23)}{=} \min \left(\frac{\|i\|_2^2}{(t+s)}, \pi \right) \\
 &\stackrel{(15)}{=} \alpha_{t+s}(i).
 \end{aligned} \tag{26}$$

Thus,

$$b_t(i) \dot{+} b_s(i) \stackrel{(17)}{=} R_{\mu,x}((\alpha_t \square \alpha_s)(i)) \stackrel{(27)}{=} R_{\mu,x}(\alpha_{t+s}(i)) \stackrel{(14)}{=} b_{t+s}(i).$$

References

- [1] G. Matheron. *Random sets and integral geometry [by] G. Matheron*. Wiley New York, 1974.
- [2] J. Serra. *Image Analysis and Mathematical Morphology*. Academic Press, Inc., USA, 1983.
- [3] J. Serra. *Image Analysis and Mathematical Morphology. Volume 2: Theoretical Advances*. Academic Press, Inc., 1988.
- [4] P. Soille. *Morphological Image Analysis: Principles and Applications*. Springer-Verlag, Berlin, Heidelberg, 2 edition, 2003.
- [5] S. Sternberg. Grayscale morphology. *Computer Vision, Graphics, and Image Processing*, 35(3):333–355, 1986.
- [6] C. Ronse. Why mathematical morphology needs complete lattices. *Signal Processing*, 21(2):129–154, 1990.
- [7] J. Goutsias, H. Heijmans, and K. Sivakumar. Morphological operators for image sequences. *Comput. Vis. Image Underst.*, 62:326–346, 1995.
- [8] Y-D. Zhang, Z. Dong, S-H. Wang, X. Yu, X. Yao, Q. Zhou, H. Hu, M. Li, C. Jiménez-Mesa, J. Ramirez, F.J. Martinez, and J.M. Gorriz. Advances in multimodal data fusion in neuroimaging: Overview, challenges, and novel orientation. *Information Fusion*, 64:149–187, 2020.
- [9] Y. Zhang, S. Wang, K. Xia, Y. Jiang, and P. Qian. Alzheimer’s disease multiclass diagnosis via multimodal neuroimaging embedding feature selection and fusion. *Information Fusion*, 66:170–183, 2021.
- [10] Zuo Y. and R. Serfling. General notions of statistical depth function. *The Annals of Statistics*, 28(2):461 – 482, 2000.
- [11] S. Velasco-Forero and J. Angulo. Random projection depth for multivariate mathematical morphology. *IEEE Journal of Selected Topics in Signal Processing*, 6(7):753–763, 2012.
- [12] R. Y. Liu and K. Singh. Ordering Directional Data: Concepts of Data Depth on Circles and Spheres. *The Annals of Statistics*, 20(3):1468 – 1484, 1992.
- [13] G. Pandolfo, D. Paindaveine, and G. Porzio. Distance-based depths for directional data. *Canadian Journal of Statistics*, 46, 09 2017.
- [14] C. Ley, C. Sabbah, and T. Verdebout. A new concept of quantiles for directional data and the angular Mahalanobis depth. *Electronic Journal of Statistics*, 8(1):795 – 816, 2014.
- [15] E. García-Portugués, D. Paindaveine, and T. Verdebout. On optimal tests for rotational symmetry against new classes of hyperspherical distributions. *Journal of the American Statistical Association*, 115(532):1873–1887, 2020.

- [16] J.B.T.M. Roerdink. Mathematical morphology on the sphere. In Murat Kunt, editor, *Visual Communications and Image Processing '90: Fifth in a Series*, volume 1360, pages 263 – 271. International Society for Optics and Photonics, SPIE, 1990.
- [17] R. A. Peters II. Mathematical morphology for angle-valued images. In Edward R. Dougherty and Jaakko T. Astola, editors, *Nonlinear Image Processing VIII*, volume 3026, pages 84 – 94. International Society for Optics and Photonics, SPIE, 1997.
- [18] A.G. Hanbury and J. Serra. Morphological operators on the unit circle. *IEEE Transactions on Image Processing*, 10(12):1842–1850, 2001.
- [19] J. Frontera-Pons and J. Angulo. Morphological operators for images valued on the sphere. In *2012 19th IEEE International Conference on Image Processing*, pages 113–116, 2012.
- [20] J. Angulo. Morphological Scale-Space Operators for Images Supported on Point Clouds. In Springer-Verlag Berlin Heidelberg, editor, *5th International Conference on Scale Space and Variational Methods in Computer Vision*, volume LNCS 9087 of *Proc. of SSVM'15 (5th International Conference on Scale Space and Variational Methods in Computer Vision)*, Lège-Cap Ferret, France, June 2015.
- [21] N.I. Fisher, T. Lewis, and B.J.J. Embleton. *Statistical Analysis of Spherical Data*. Cambridge University Press, 1987.
- [22] P. Jackway. Morphological scale-spaces. In Peter W. Hawkes, editor, *Morphological Scale-Spaces*, volume 99 of *Advances in Imaging and Electron Physics*, pages 1–64. Elsevier, 1997.
- [23] H.J.A.M. Heijmans. *Morphological Image Operators*. Advances in electronics and electron physics: Supplement. Academic Press, 1994.
- [24] L. E. Blumenson. A derivation of n-dimensional spherical coordinates. *The American Mathematical Monthly*, 67(1):63–66, 1960.
- [25] J. W. Tukey. Mathematics and the picturing of data. In *Proceedings of the International Congress of Mathematicians (Vancouver, B. C., 1974)*, volume 2, page 523–531, 1975.
- [26] R. Liu. On a Notion of Data Depth Based on Random Simplices. *The Annals of Statistics*, 18(1):405 – 414, 1990.
- [27] D. Donoho and M. Gasko. Breakdown properties of location estimates based on halfspace depth and projected outlyingness. *Ann. Stat.*, 20, 12 1992.
- [28] Y. Vardi and C. Zhang. The multivariate 11-median and associated data depth. *Proceedings of the National Academy of Sciences of the United States of America*, 97:1423–6, 03 2000.
- [29] N. I. Fisher. Spherical medians. *Journal of the Royal Statistical Society. Series B (Methodological)*, 47(2):342–348, 1985.
- [30] J. Angulo. Morphological colour operators in totally ordered lattices based on distances: Application to image filtering, enhancement and analysis. *Computer Vision and Image Understanding*, 107:56–73, 07 2007.
- [31] E. Aptoula and S. Lefèvre. A Comparative Study on Multivariate Mathematical Morphology. *Pattern Recognition*, 40(11):2914–2929, March 2007.
- [32] V. Barnett. The ordering of multivariate data. *Journal of the Royal Statistical Society. Series A (General)*, 139(3):318–355, 1976.
- [33] L. Najman and H. Talbot. *Mathematical Morphology: from theory to applications*. ISTE-Wiley, June 2010. ISBN: 9781848212152 (520 pp.).
- [34] H.J.A.M. Heijmans and R. van den Boomgaard. Algebraic framework for linear and morphological scale-spaces. *Journal of Visual Communication and Image Representation*, 13(1):269–301, 2002.
- [35] T. Strömberg. *The operation of infimal convolution*. Instytut Matematyczny Polskiej Akademii Nauk, 1996.
- [36] S. Kappenthuler and S. Seeger. Assessing the long-term potential of fiber reinforced polymer composites for sustainable marine construction. *Journal of Ocean Engineering and Marine Energy*, 7, 05 2021.
- [37] Tin Barišin, Katja Schladitz, Claudia Redenbach, and Michael Godehardt. Adaptive morphological framework for 3d directional filtering. *Image Analysis & Stereology*, 41(1), 2022.
- [38] O. Wirjadi, M. Godehardt, K. Schladitz, B. Wagner, A. Rack, M. Gurka, S. Nissle, and A. Noll. Characterization of multilayer structures in fiber reinforced polymer employing synchrotron and laboratory x-ray ct. *International Journal of Materials Research*, 105(7):645–654, 2014.
- [39] O. Wirjadi, K. Schladitz, P. Easwaran, and J. Ohser. Estimating fibre direction distributions of reinforced composites from tomographic images. *Image Analysis & Stereology*, 35(3):167–179, 2016.

- [40] T. Nogatz, C. Redenbach, and K. Schladitz. 3d optical flow for large ct data of materials microstructures. *Strain*, page e12412, 2021.